Plant Molecular Biology (2018) 97:421–433
https://doi.org/10.1007/s11103-018-0748-3

FZL is primarily localized to the inner chloroplast membrane however influences thylakoid maintenance

Manali Patil[1,2] · Stephanie Seifert[1] · Franka Seiler[1] · Jürgen Soll[1,2] · Serena Schwenkert[1]

Received: 18 December 2017 / Accepted: 5 June 2018 / Published online: 27 June 2018

Abstract

Key message **FZL is primarily localized to the chloroplast inner envelope and not to the thylakoids, but nevertheless affects the maintenance of thylakoid membranes and photosynthetic protein complexes.**

Abstract The fuzzy-onion-like protein (FZL) is a membrane-bound dynamin-like GTPase located in the chloroplast. We have investigated the chloroplast sub-localization of the endogenous FZL protein and found it to be primarily localized to the inner envelope. Moreover, we observed that mature leaves of *fzl* mutants start to turn pale, especially in the midvein area of the leaves, 11 days after germination. We therefore assessed their photosynthetic performance as well as the accumulation of thylakoid membrane proteins and complexes after the initial appearance of the phenotype. Interestingly, we could observe a significant decrease in amounts of the cytochrome b_6f complex in 20-day-old mutants, which was also reflected in an impaired electron transport rate as well as a more oxidized P700 redox state. Analysis of differences in transcriptome datasets obtained before and after onset of the phenotype, revealed large-scale changes in gene expression after the phenotype became visible. In summary, we propose that FZL, despite its localization in the inner chloroplast envelope has an important role in thylakoid maintenance in mature and aging leaves.

Keywords Chloroplast · Dynamin-like protein · Inner envelope · Thylakoid · *Arabidopsis*

Introduction

The fuzzy-onion-like protein (FZL) is a dynamin-like GTPase, which is closely related to the mitochondrial fusion protein, FZO/mitofusin. FZO is conserved across the fungal and animal kingdom. It localizes to the outer membrane of mitochondria and is thought to mediate tethering of mitochondrial outer membranes via its coiled coil domains, which are exposed to the cytosol and can interact with tethering factors on the same and opposing mitochondrial membranes. Its deletion leads to fragmented mitochondria due to defects in fusion (Mozdy and Shaw 2003; van der Bliek et al. 2013). Interestingly, *FZL* is the only *FZO*-like gene found in the *Arabidopsis* genome. However, FZL contains an N-terminal chloroplast targeting sequence and is localized to chloroplasts, as has been shown by the expression of a FZL–GFP fusion protein (Gao et al. 2006). The overexpressed FZL–GFP fusion protein was detected in thylakoids as well as in the envelopes of chloroplasts in *Arabidopsis*. Moreover, it has been shown that T-DNA insertion *fzl* mutants in the Columbia-0 (Col-0) background develop pale green leaves and accumulate fewer, but larger, chloroplasts. Ultrastructural analysis of these chloroplasts has revealed that the morphology of the thylakoids differs from that observed in wild type (WT). Intriguingly, larger numbers of vesicles have also been observed in *fzl* chloroplasts, leading to the initial hypothesis that FZL might be involved in thylakoid biogenesis or maintenance, possibly by promoting vesicle transport from the inner chloroplast envelope (Gao et al. 2006; Waters and Langdale 2009). Further support for a role of FZL in membrane fission or fusion came from the studies on its closest cyanobacterial homolog of

Electronic supplementary material The online version of this article (https://doi.org/10.1007/s11103-018-0748-3) contains supplementary material, which is available to authorized users.

✉ Serena Schwenkert
serena.schwenkert@lmu.de

[1] Department Biologie I, Botanik, Ludwig-Maximilians-Universität, Großhaderner Strasse. 2-4, 82152 Planegg-Martinsried, Germany

[2] Munich Center for Integrated Protein Science CiPSM, Ludwig-Maximilians-Universität, Feodor-Lynen-Strasse 25, 81377 Munich, Germany

FZL, bacterial dynamin-like protein (BDLP). The function of BDLP has been analyzed by electron cryo-electron microscopical reconstruction of coated lipid tubes, which suggested a role for the protein in mediating membrane curvature. (Low and Lowe 2006; Low et al. 2009).

Strikingly, in contrast to the pale green phenotype observed in *fzl* mutants in Col-0 background, two independent studies have described *fzl* mutants in *Landsburg erecta* (Ler) background, which display a lesion mimic mutant (LMM) phenotype (Landoni et al. 2013; Tremblay et al. 2016). Typically, the LMM phenotype is associated with constitutively active hypersensitive cell death and defense responses, which are activated in WT not only upon entry into senescence, but also as a reaction to abiotic and biotic stresses, such as pathogen attack (Landoni et al. 2013). Cell death mediated by FZL was reported to be dependent on salicylic acid and the expression of several defense and autophagy related genes was found to be upregulated in *fzl* (Ler) (Tremblay et al. 2016). The severity of the LMM phenotype is modulated by environmental conditions such as temperature, humidity and light, in addition to variations in the genetic background. In case of *fzl* (Ler) mutants, exposure to high temperature (28 °C) or low light treatments (50 µmol m^{-2} s^{-1}) was shown to rescue the LMM phenotype. However, the plants nevertheless remained pale green, just like *fzl* (Col-0) mutants (Landoni et al. 2013).

In this work we studied the impact of FZL with respect to its impact on photosynthesis and the formation of thylakoid membrane complexes in Col-0 plants. We show that FZL is primarily localized to the chloroplast inner envelope and not to the thylakoids, but nevertheless seems to affect the maintenance of thylakoid membranes and photosynthetic protein complexes. We observed that *fzl* mutant leaves turn pale after 11–13 days post germination. Therefore, we investigated the accompanying changes in the transcript levels by analyzing the transcriptomes before and after the appearance of the pale green leaf phenotype.

Results

Lack of FZL induces the emergence of a pale green phenotype 11 days post germination

Three homozygous Col-0 mutants bearing independent T-DNA insertions in the *FZL* gene were isolated (Fig. 1a and Online Resource 1). The leaves of *fzl* plants displayed a pale green phenotype, predominantly appearing in the mid vein region, especially when the mutants were grown under LED lights (22 °C, 200 µmol m^{-2} s^{-1} light, long day conditions). The phenotype first became manifest in 11 to 13-day-old plants (Fig. 1b). A specific polyclonal antiserum raised against FZL was used to confirm the knockout of *FZL* function at the protein level. It recognized a band of approximately 95 kDa, corresponding to the mature FZL protein in both Col-0 and as the backcrossed WT line, which was absent in the insertion mutants (Fig. 1c). Since the phenotype was identical in all three mutant lines (Online Resource 1) further experiments were performed with *fzl-1* grown in LED light focusing on the midvein area of the leaves (Fig. 1d). To strengthen the observation that the mutant leaves turned paler from day 11 onwards, we measured the chlorophyll content at day 10, day 13 and day 20. Whereas no significant change was visible in 10-day-old plants, the chlorophyll content starts to decrease after 13 days to 78.6% of WT levels and is significantly decreased to 76% of WT levels in 20-day-old plants (Fig. 1e and Online Resource 2).

FZL is primarily localized to the inner envelope of chloroplasts

An *Arabidopsis* line overexpressing a FZL–GFP fusion protein was previously generated by Gao *et al*. Using fluorescence microscopy and immunoblotting with anti-GFP antibodies, FZL–GFP was shown to be detectable in both the chloroplast envelope and the thylakoid membrane (Gao et al. 2006). We determined the sub-chloroplast localization of the endogenously expressed FZL using the FZL specific antiserum. Chloroplasts isolated from *Pisum sativum* were fractionated into outer and inner envelope, stroma and thylakoids and these samples were subjected to western analysis (Fig. 2a, Online Resource 1 shows an alternative set of western blots). Surprisingly, FZL was detected exclusively in the inner envelope fraction (Fig. 2a, upper panel, Online Resource EMS_1). Antisera raised against Toc64, Tic110 (and Tic40 in Online Resource 1), FBPase and D1 served as marker protein controls for outer envelopes, inner envelopes, stroma and thylakoids, respectively, and confirmed the purity of the fractions (Fig. 2a, lower panels, Online Resource EMS_1). We therefore conclude that FZL is primarily localized to the inner envelope of chloroplasts.

In silico analysis with TargetP predicted that FZL is localized to chloroplasts and/or mitochondria. We therefore probed western blots bearing *Arabidopsis* mitochondrial membranes and chloroplast inner envelopes from pea with the antiserum against FZL. An antiserum against the mitochondrial protein CoxII was used as control, as well as against Tic110 for inner envelopes. FZL could be detected exclusively in the inner envelope of chloroplasts but not in the mitochondria (Fig. 2b), in agreement with previous reports based on FZL–GFP/YFP expression (Gao et al. 2006; Tremblay et al. 2016).

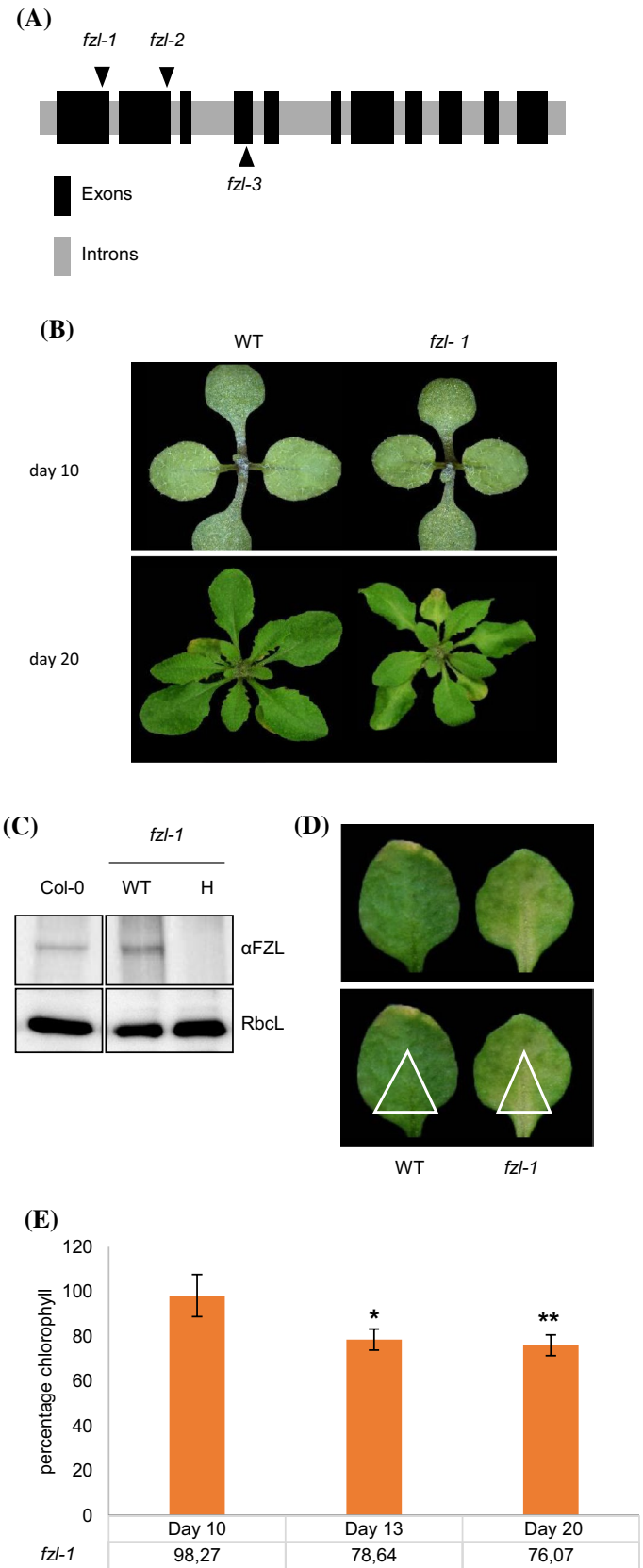

Fig. 1 Phenotype of *fzl* mutant plants grown under LED light. **a** The T-DNA insertion sites mapped to the *FZL* gene in the three Salk *fzl* lines are indicated by the black arrowheads (black, exons; grey, introns). **b** Phenotype of *fzl-1* mutants grown under long day conditions at 200 µM m^{-2} s^{-1} LED light. Top panel, 10 day-old *fzl-1* mutants with phenotype similar to WT. Bottom panel, 20 day-old *fzl-1* mutants when grown in high light show a stronger pale green phenotype especially at the mid rib region compared to WT. **c** Immunoblot analysis of *fzl-1* line using anti FZL antisera (upper panel). 15 µg of total protein loaded on a 10% SDS gel. Lower panel, equal loading is shown by the antisera's cross reactivity with Ribulose-1,5-bisphosphatase (RbcL). H, homozygous mutant; WT, backcrossed WT. **d** 20-day-old WT and *fzl* leaf (upper panel). The leaf material near the mid-vein region that was used for analysis of the levels of photosynthetic efficiency, levels of proteins by immunoblotting, BN-PAGE and microarray experiment is shown enclosed into a triangle (lower panel). **e** Chlorophyll concentration was measured using leaves from 10, 13 and 20-day-old plants grown in LED light, *P*-value ≥ 0.00001, n ≥ 4

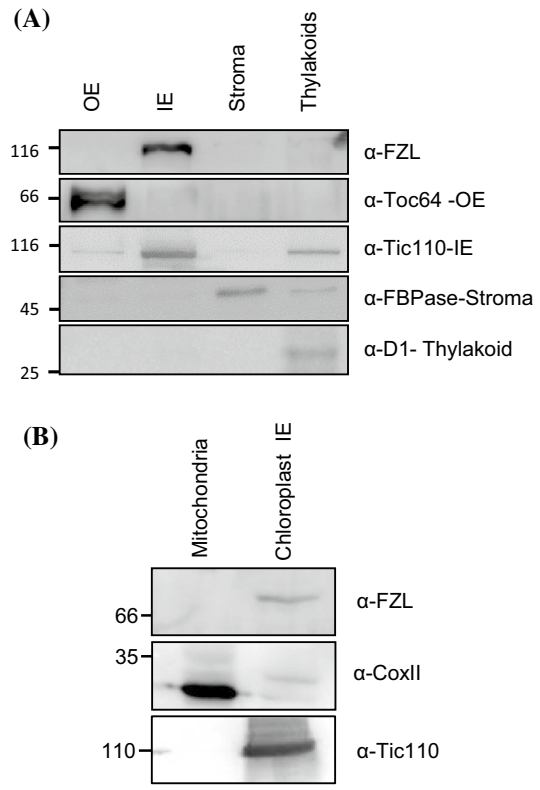

Fig. 2 FZL is localized in inner envelope of chloroplast and not mitochondria. **a** Isolated pea chloroplasts were fractionated into inner envelopes, outer envelopes, thylakoid membranes and a stroma and samples (equivalent to 15 µg protein) were loaded on a 12% SDS gel. After electrophoresis and membrane transfer, blots were probed with the anti-FZL antiserum. Antibodies against the outer envelope protein TOC64, inner-envelope protein Tic110, the soluble stromal protein FBPase and the thylakoid membrane protein D1 were used as controls. **b** FZL is not present in mitochondria. Purified *Arabidopsis* mitochondria (50 µg protein) and chloroplast inner envelope fraction (15 µg protein) was loaded on a 10% SDS gel and were electrophoresed, blotted and probed with anti-FZL as described as described above. An antibody against the mitochondrial protein CoxII was used as control, as well as against the inner envelope protein Tic110

Lack of FZL alters accumulation of thylakoid membrane proteins and photosynthetic activity

As a next step, we analysed the levels of thylakoid membrane proteins in 10-day-old as well as 20-day-old WT and *fzl* mutants by immunoblotting and tested subunits of PSII (CP47, D1), PSI (PsaF), the cytochrome b_6f complex (Cyt*f* and Cytb_6) and the ATP synthase (CF_1-α/β) (Fig. 3a, b). Interestingly, in 10-day-old plants, hardly any changes of the levels of thylakoid proteins were visible in the mutant (Fig. 3a). However, in 20-day-old plants more obvious changes were observed. Although only a marginal reduction could be detected in the protein levels of CP47 and PsaF in *fzl* plants, Cyt*f* and D1 were reduced by approximately 50% in comparison to WT levels, Cytb_6 by even 75%, while amount of the ATP synthase was slightly increased (Fig. 3a, b). We further analysed whether formation of the photosynthetic complexes was affected, by separating the solubilized protein complexes on a Blue-Native (BN)-PAGE. Therefore, thylakoid membranes were isolated from the midvein sections of WT and *fzl* mutants and equal amount of protein was loaded and separated on a 5–15% BN gel after solubilizing the membrane complexes in 1% dodecyl-β-D-maltoside. Indeed, the band corresponding to the PSII monomer/cytochrome b_6f complex was slightly reduced in the *fzl* mutant as compared to WT (Fig. 3c). These results indicate that lack of FZL impairs the efficiency of photosynthetic electron transport, caused by reduced levels of Cyt b_6f complex proteins in the mid-vein region.

Since we observed changes in the levels of photosynthetic complexes, we aimed to assess the efficiency of the photosynthetic performance and the levels of thylakoid membrane proteins in the *fzl* mutant. We focused on the midvein region of the leaves, which displayed the pale green phenotype most prominently (Fig. 1d). The photosynthetic performance was analysed by measuring the maximum quantum efficiency F_v/F_m in the dark-adapted state, based on chlorophyll *a* fluorescence (Fig. 4a). In 10-day-old plants, the F_v/F_m in *fzl* mutants and WT was comparable. However, in 20-day-old plants, the F_v/F_m in the mutant was slightly reduced (0.6) relative to WT (0.75) (Fig. 4b). The electron transfer rate (ETR) from PSII to downstream components of the photosynthetic electron transport chain was measured at different levels of illumination with photosynthetically active radiation (PAR). Again, no significant difference was observed in the ETRs of WT and 10-day-old *fzl* mutant leaves (Fig. 4c). However, the ETR in 20-day-old *fzl* mutants was found to decrease significantly with increasing light (PAR) intensities relative to WT, indicating a main functional impairment of the photosynthetic apparatus downstream of PSII (Fig. 4d). In order to additionally monitor the photosynthetic electron flow through PSI, we estimated the redox state of P700 in the light by measuring oxidation of P700. P700 was partially oxidized to $P700^+$ at actinic light of 200 µmol m^{-2} s^{-1} (ΔA), then reduced in the dark and subsequently oxidized to a maximum level of $P700^+$ under far-red light illumination (ΔA_{max}). The P700 oxidation ratio ($\Delta A/\Delta A_{max}$) was calculated in WT and *fzl* plants (Table 1). The redox state of P700 was found to be significantly more oxidized in the mutant (a ratio of 0.73 in 20-day-old *fzl* mutants and 0.49 in the WT), which could again indicate an impairment in the cytochrome b_6f complex function.

An impairment of the cytochrome b_6f complex followed by a decreased proton translocation into the lumen, would usually be expected to result in a reduced non-photochemical quenching (qN), as has been observed previously (Hojka et al. 2014; Schottler et al. 2007; Yamori et al. 2011). Surprisingly however, we observed that qN

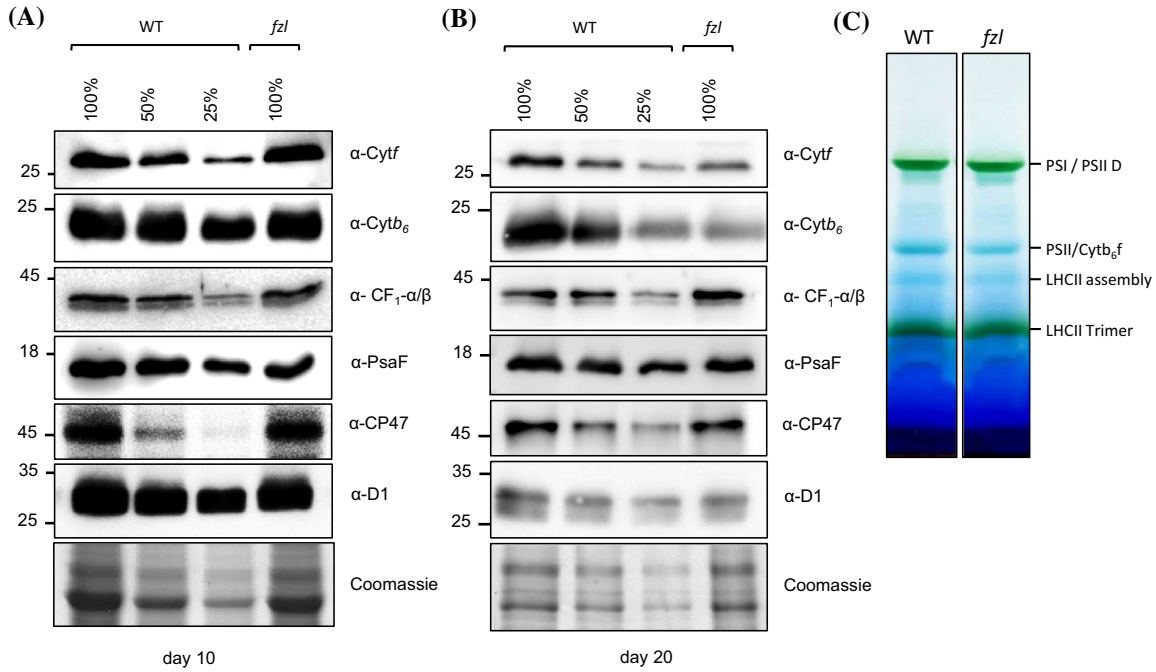

Fig. 3 Accumulation of thylakoid membrane proteins. **a** and **b** Total membrane proteins isolated from the midrib region of leaves from 10-day-old (**a**) and 20 day-old (**b**) plants grown under LED light were loaded on a 12% SDS gel, fractionated, blotted and probed with antibodies against proteins of the cytochrome b_6f complex, the ATP synthase, PSI and PSII. 100% protein equals 10 µg of protein. **c** Thylakoids of WT and *fzl* plants were isolated from the midrib region of leaves from 20 day-old plants grown under LED light, solubilized in 1% β-dodecylmaltoside and photosynthetic complexes were separated by BN-PAGE

was even higher in 20-day-old mutants as compared to the WT, i.e. 0.80 in 20-day-old *fzl* mutants versus 0.65 in the WT at 200 µmol m^{-2} s^{-1} actinic light (Table 1). Additionally, we measured the net re-reduction rate of P700 in the WT and *fzl* mutants after oxidation of P700 with far-red light. The re-reduction rate was measured in the dark via its exponential decay. The mean value of the half-time of P700 re-reduction ($t_{1/2}$) was significantly lower in the *fzl* mutant (0.47 s) compared to the WT (0.65 s) (Table 1), indicating that light-independent reduction of the plastoquinone pool via non-photochemical processes is increased by approx. 28% in the mutant.

Analysis of changes in transcript levels upon the onset of the fzl phenotype

To identify genes that are differentially regulated in the *fzl* mutant relative to WT, which could further help to elucidate the probable role of FZL, a global transcriptomic study was performed. Given that the phenotype first appears at the age of 11–13 days, samples were prepared from the area around the mid-vein of leaves obtained from 10-day-old to 13-day-old mutant and WT plants (Fig. 1b). Biotinylated cRNA was fragmented and hybridized to GeneChip *Arabidopsis* ATH1 arrays and results were further analyzed as described in Materials and Methods.

At day 10, 1107 genes were found to be up regulated and 955 genes were down regulated in *fzl* compared to WT (Fig. 5a). Interestingly, these numbers had increased significantly by day 13, at which time 3397 genes were upregulated and 3570 down regulated in the mutant (Fig. 5b). Note that, in addition to the very considerable increase in the total number of differentially regulated genes (DEGs), down-regulated genes outnumber the genes up-regulated in the mutant (as compared to WT) at the later time-point (Fig. 6 and Online Resource 4).

The genes identified belonged to various gene ontology (GO) molecular function categories as annotated based on Mapman BINs (Usadel et al. 2009) (Fig. 6). Genes related to tetrapyrrole synthesis were deregulated as expected from the low amounts of chlorophyll found in *fzl* plants. However, surprisingly photosystem and light reaction related genes, especially light those for harvesting complex (LHCs) proteins where up-regulated. Therefore, we decided to validate these differences at the protein level by immunoblotting using antisera directed against LHCa (LHCa1, LHCa2 and Lhca4) and LHCb (Lhcb1, Lhcb2 and Lhcb4) proteins and PORB (protochlorophyllide oxidoreductase B, chlorophyll metabolism) (Fig. 7a, b, upper panel). No significant differences were found at the protein levels of LHCs and PORB with the exception of LHCa1 protein which was slightly increased. Moreover, there were considerable variations in transcription levels of genes

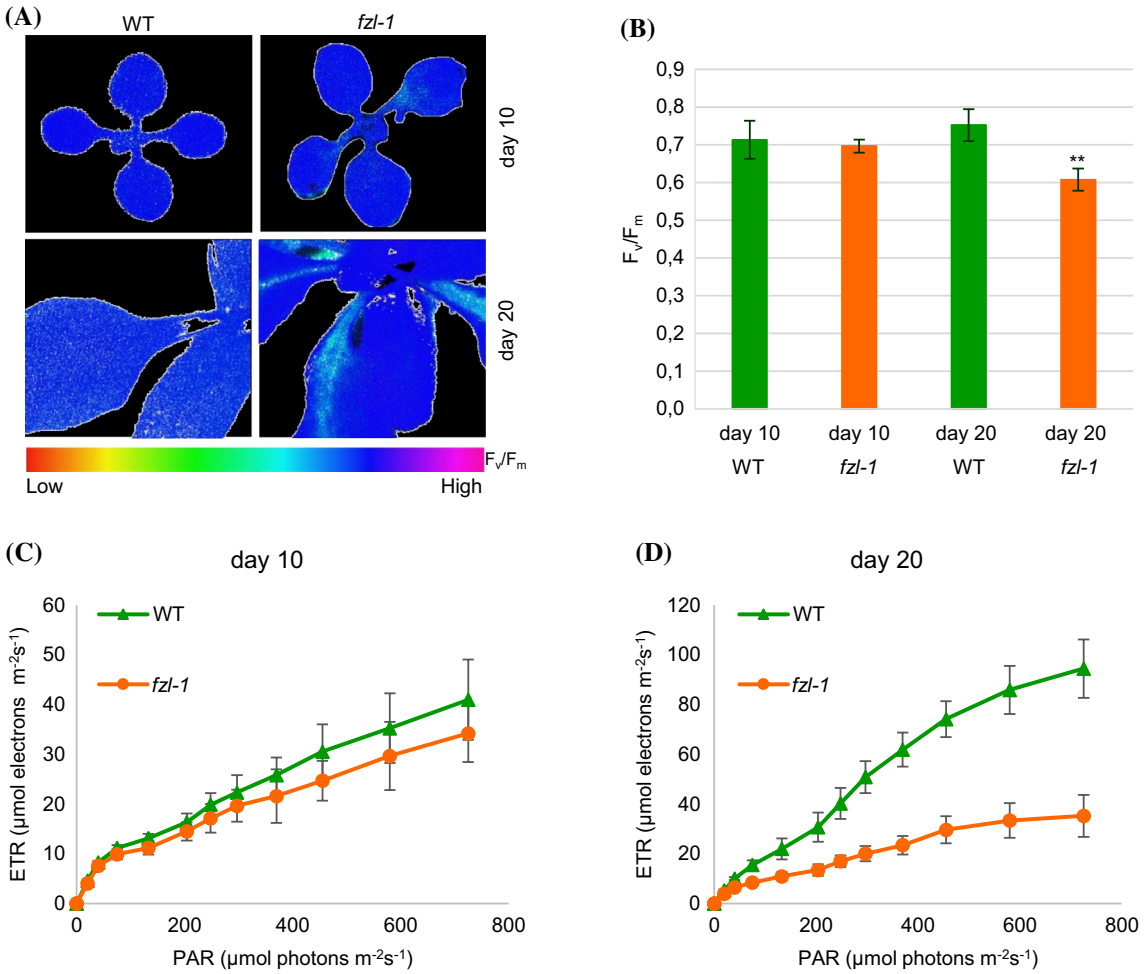

Fig. 4 Photosynthetic performance of *fzl* mutants. **a** Photosynthetic performance of *fzl* mutants is reduced in comparison to WT. F_v/F_m of *fzl* mutants and WT plants monitored using an Imaging PAM system at day 10 (top panel) and day 20 (bottom panel) after germination. The colour scale indicates the relative photosynthetic activity with red being the lowest and magenta being highest F_v/F_m values. **b** Quantification of F_v/F_m measurements as shown in **a**, *P*-value: 2.86336E−07, $n \leq 9$. **c** and **d** Quantification of electron transfer rate (ETR) measured at increasing light intensities on day 10 (**c**) and day 20 (**d**), $n \leq 9$

Table 1 Photosynthetic parameters of the WT and *fzl* mutant

	qN[a]	$t_{1/2}$ P700 red[b]	P700 ox ratio[c]
WT day 10	0.79 ± 0.02	n.a.	n.a.
fzl day 10	0.78 ± 0.01	n.a.	n.a
WT day 20	0.65 ± 0.14	0.65 ± 0.05	0.46 ± 0.09
fzl day 20	0.80 ± 0.04	0.47 ± 0.05	0.73 ± 0.05

[a]Non-photochemical quenching at 200 µmol m^{-2} s^{-1} actinic light

[b]Half-time of non-photochemical P700 re-reduction in the dark (s), P700 oxidation ratio in ($\Delta A/\Delta A_{max}$) at 200 µmol m^{-2} s^{-1}, $n \geq 5$

involved in carbohydrate metabolism, with 14 members of this category being down-regulated and 5 genes up-regulated by at least twofold. Therefore, we analyzed the levels of the enzymes triose-phosphate isomerase (TIP), glyceraldehyde-3-phosphate dehydrogenase (GAPC1), succinate dehydrogenase (SDH4) and glucose-6-phosphate dehydrogenase (G6PDH), all of which were found to be down-regulated at the transcriptional level on day 13 in *fzl* in the microarray experiment. Amounts of the SDH4 protein were found to be reduced in the *fzl* mutant as compared to WT, whereas GAPC1 and G6PDH levels were increased in *fzl* despite declines in the steady-state amounts of the corresponding transcripts. There was no change in levels of TIP (Fig. 7b). This discrepancy is not surprising given that transcript and protein levels and lifetimes are regulated by different mechanisms and can vary significantly from each other.

Discussion

Fzl mutants in Col-0 background were previously reported to have pale green leaves and fewer, but larger, chloroplasts which also showed changes in the organization of grana

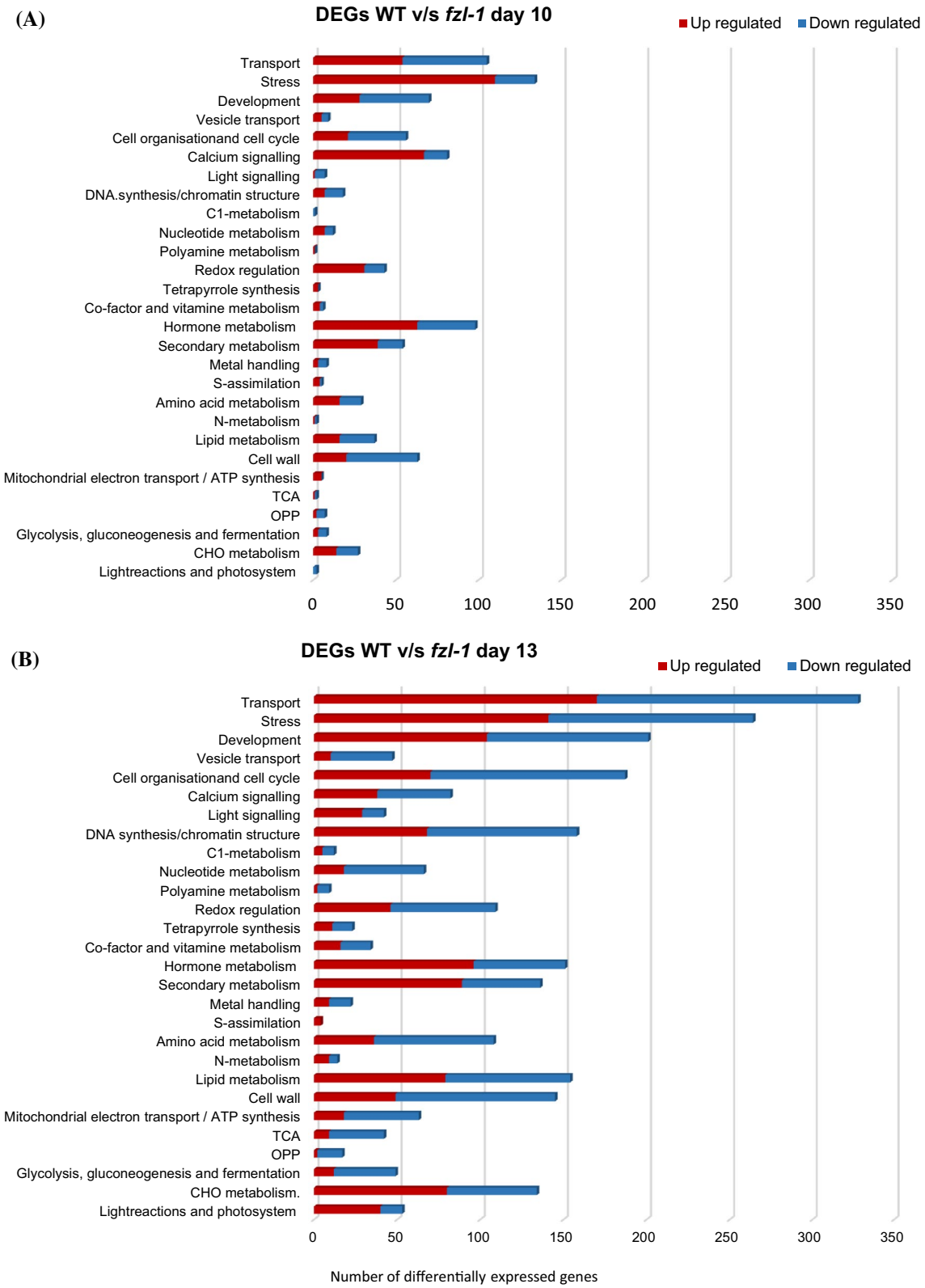

Fig. 5 Number of differentially expressed genes of various GO molecular function categories. The graphs show the numbers of genes differentially regulated in *fzl* relative to WT on day 10 (**a**) and day 13 (**b**) that were assigned to the indicated GO molecular function categories

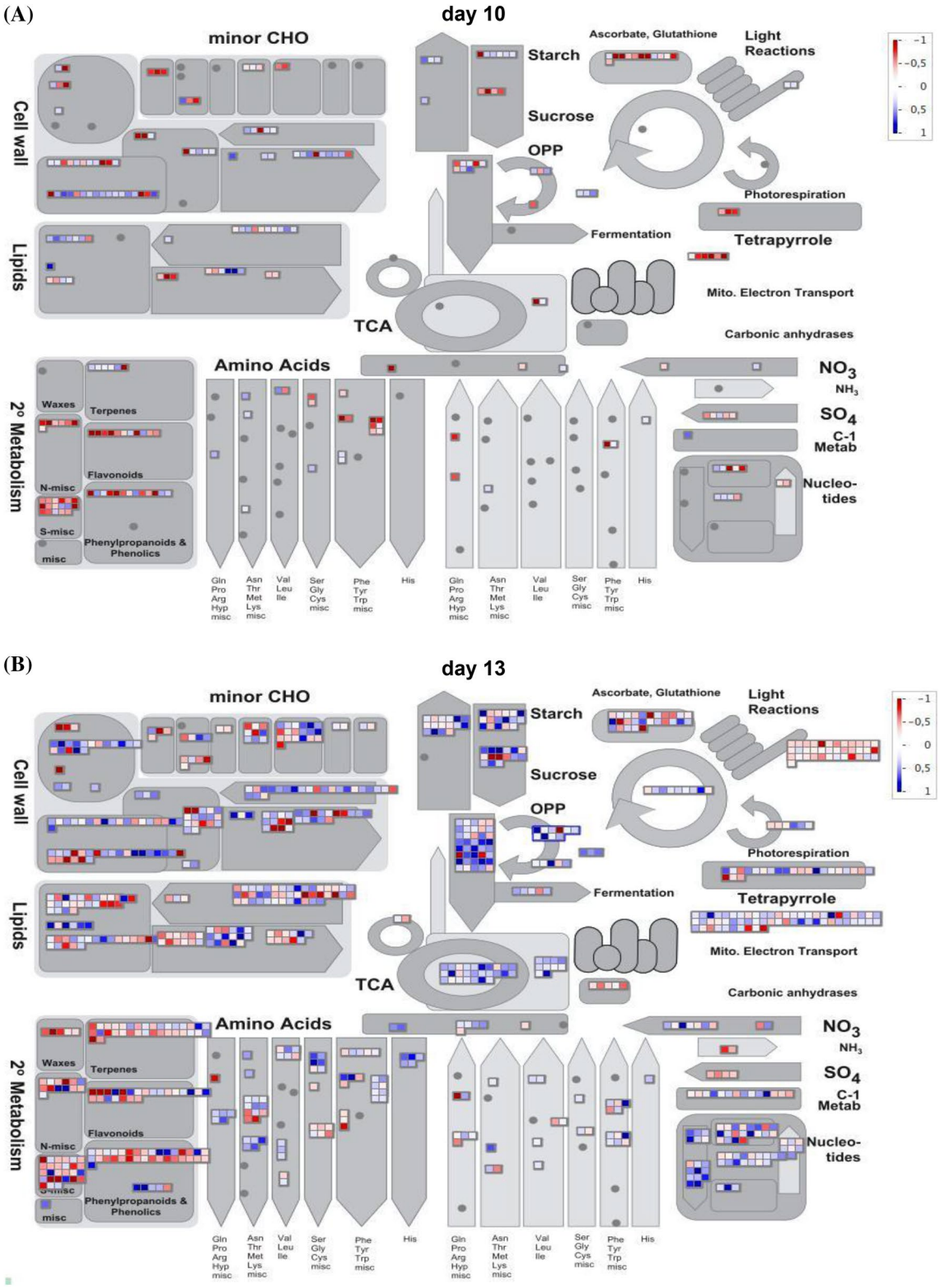

Fig. 6 Differentially regulated genes as annotated based on Mapman BINs. Differentially regulated genes in *fzl* as compared to WT annotated to various GO molecular function categories as on day 10 (**a**) and day 13 (**b**)

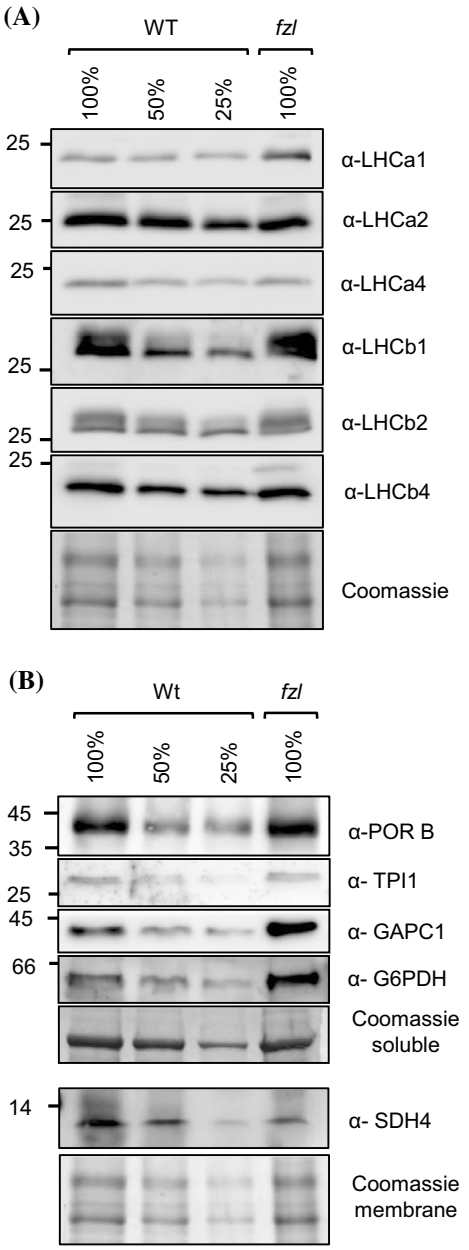

Fig. 7 Quantification of protein products of selected differentially expressed genes. Levels of light-harvesting-complex proteins (LHCs) (**a**) and products of chlorophyll- and carbohydrate-metabolism-related genes (**b**) that are differentially regulated in *fzl* relative to WT were determined by immunoblot analysis with cognate antibodies. Total membrane or soluble protein fractions electrophoresed on a 12% SDS gel and immunodecorated. 100% protein equals 10 µg. *PORB* protochlorophyllide oxidoreductase B; *TIP* triose-phosphate isomerase; *GAPC1* glyceraldehyde-3-phosphate dehydrogenase; *SDH4* succinate dehydrogenase; *G6PDH* glucose-6-phosphate dehydrogenase

stacks and stroma lamellae in thylakoids (Gao et al. 2006). Since no differences in total lipid and/or fatty acid composition were observed in *fzl* relative to WT, the changes in chloroplast size were considered to be a secondary effect and the function of *fzl* remained unclear.

We analyzed three independently derived T-DNA insertion lines for *fzl* and all three showed a pale green phenotype from 11 to 13 days onwards, which was even more pronounced when plants were grown under grown under 200 µmol m^{-2} s^{-1} LED light, which was also evident when analyzing the chlorophyll content (Fig. 1 and Online Resource 1). Interestingly, there was no visible phenotype observed in younger plants (up to 10 days). We measured the average diameter of chloroplasts in protoplasts isolated from WT and *fzl* leaves, which was higher in all the mutant lines, in agreement with the earlier observation (Online Resource 3) (Gao et al. 2006; Landoni et al. 2013). Further, we quantified the amount of chlorophyll and found it to be significantly reduced to 70% of the WT value, when grown under 100 µmol m^{-2} s^{-1} normal light in 25 day-old plants (Online Resource 3).

Goa et al. have generated an *Arabidopsis* line overexpressing a FZL–GFP fusion protein and found it to be localized to chloroplasts. Moreover, with increasing expression levels, FZL–GFP puncta could be seen at the envelope as well as inside the chloroplast. Subsequently, they subfractionated chloroplasts from these lines and showed that FZL–GFP is localized to both the chloroplast inner envelope and the thylakoid membrane using a GFP-specific antibody (Gao et al. 2006). However, only the localization of the overexpressed FZL–GFP was analyzed, not that of the endogenous FZL protein. Therefore, we raised a FZL specific antibody to detect the endogenously expressed FZL and found that it was exclusively present in the inner envelope of the chloroplast based on tests with pea chloroplast subfractions. (Fig. 2a). The discrepancy with the results of Gao et al. could be due to miss-localization of GFP tagged FZL owing to its overexpression.

FZL is the only homologue of the mitochondrial fusion factor, FZO, found in plants. Although in silico analysis predict FZL to be localized to chloroplasts and/or mitochondria, we were unable to detect endogenous FZL in mitochondria by immunoblotting with FZL antisera, thus confirming earlier observations using fluorescence tagged FZL (Gao et al. 2006; Tremblay et al. 2016).

Surprisingly, we observed that the phenotype of *fzl* became apparent in mature leaves after approx. 11–13 days post germination. Consequently, we tested of the accumulation of thylakoid membrane proteins revealed that the levels of cytochrome b_6f (Cyt*f* and Cytb_6) complex proteins as well as D1 were significantly reduced in 20-day-old plants, although steady-stale concentrations of PSI (PsaF) and PSII (D1and CP47) components were only slightly reduced. Levels of the ATP synthase (CF_1-α/β), on the other hand, marginally higher. Similar effects have previously been noted in mutants of low molecular weight subunits of the cytochrome b_6f complex (PetL, PetG, and PetN) (Schwenkert et al. 2007). Interestingly, no significant changes were observed

in younger, 10-day-old plants, showing that the phenotype is age dependant (Fig. 3).

Photosynthetic measurements of the ETR as well as the P700 oxidation state indicated an impairment of the electron flow from PSII to PSI. However, the observed high qN values were unexpected and did not correlate with previous results showing a reduced qN in cytochrome b_6f complex mutants (Hojka et al. 2014; Schottler et al. 2007; Yamori et al. 2011). Possibly, an overall change in enzymes levels and the corresponding metabolites could result in metabolic imbalances and thus account for the elevated qN values, although the observation is unusual. Additionally, we determined the half-time of the P700 re-reduction rate in the dark, which was significantly faster in the mutant, indicating that light-independent reduction of the plastoquinone pool is increased in the mutant.

The cytochrome b_6f complex is involved the transfer of electrons from PSII to PSI and thus functions as a rate limiting step in photosynthesis (Schottler et al. 2007). It plays a predominant role in photosynthetic flux control and consequently is involved in the redox regulation in close coordination with ATP synthase (Schottler et al. 2015). The biogenesis of the cytochrome b_6f complex is known to occur mainly in younger leaves and the turn-over rate decreases over time in mature leaves. This is in contrast to the turn-over rates of components of PSI and PSII, which remain higher in mature leaves (Schottler et al. 2007). These considerations led us to the hypothesis that loss of FZL impairs thylakoid maintenance or remodelling in mature leaves, rather that thylakoid biogenesis itself. We assume that the selective decrease in levels of the cytochrome b_6f complex in 20 day-old *fzl* mutants (when the other components of the photosynthetic electron transport chain are still largely intact) is due to these differences in turn-over rates in mature leaves.

In order to shed more light on the processes that are affected by the loss of FZL, we performed a global transcriptomic study to identify genes that are differentially regulated in the *fzl* mutant relative to WT before and after the onset of a visible phenotype. Tetrapyrrole synthesis genes were found to be significantly deregulated, which is displayed by the decrease in chlorophyll content in 13 and 20 day-old *fzl* mutants (Fig. 1e). Interestingly, genes for light-harvesting complex (LHCs) proteins were unexpectedly slightly up-regulated. However, when analyzed at the protein level, no significant change was observed at 13 days.

We also analyzed at the levels of enzymes of carbohydrate metabolism, whose coding genes were found to be down-regulated. However, despite this downregulation at the transcriptional level, GAPC1 and G6PDH protein levels were higher, TIP levels were unchanged and amounts of SDH4 were found to be reduced in the *fzl* mutant as compared to WT. This inconsistency can be accounted for by differences between regulation of mRNA transcription and protein translation processes. The dysregulation of carbon metabolism may also account for a general metabolic imbalance, which could contribute to the elevated observed non-photochemical quenching as discussed above.

In studies conducted on *fzl* mutants isolated in the *Landsberg erecta* (Ler) background, which display a LMM phenotype, FZL was reported to be responsible for regulating cell death and defence responses. The LMM phenotype persisted in heterozygotes obtained by crossing *fzl*-Col-0 with *fzl*-Ler and several senescence-, autophagy- and defense-related genes were up-regulated (Landoni et al. 2013; Tremblay et al. 2016). Although *fzl*-Col-0 does not show a specific senescence related phenotype, the defects in thylakoid membrane structure, reduced chlorophyll content and LMM phenotype in the Ler background led us to investigate whether changes in senescence-related genes might indicate a general role for FZL in this process. However, we found no significant changes in the expression patterns of senescence- and autophagy-related genes before or after the appearance of the pale green phenotype (Online Resource 4). In agreement with this finding, Landoni et al. have observed that the LMM phenotype in *fzl* (Ler) mutants can be rescued by growth at high temperature and under low light conditions, which might indicate that the defense and cell death response are a secondary effect of the loss of FZL (Landoni et al. 2013).

Since FZL is a dynamin-like GTPase and chloroplast of *fzl* mutants accumulate an increased number of vesicles, FZL has long been hypothesized to be involved in vesicle mediated thylakoid membrane biogenesis processes (Gao et al. 2006; Jilly et al. 2018; Karim and Aronsson 2014; Waters and Langdale 2009). In presence of light, chloroplasts develop from proplastids that hardly contain internal membrane structures that develop into a complex network of thylakoid membranes (Charuvi et al. 2012; Waters and Langdale 2009). Vesicles and tubules emerging from the inner envelope have been observed frequently and are thought to carry the cargo for thylakoid membrane biogenesis and/or maintenance (Jilly et al. 2018; Karim and Aronsson 2014; Waters and Langdale 2009; Westphal et al. 2001). The bacterial BDLP and FZL are related with 29% overall identity, mainly contributed by the GTPase domain, although the FZL has a longer N-terminal extension, that includes the transit peptide. We performed in silico structural prediction analysis by one to one threading of FZL (288–912 aa) based on the GDP bound BDLP protein structure. The results show that the structures are highly similar with 100% confidence (Online Resource 5). This indicates that FZL could act in similar way mediating membrane fission or fusion. Moreover, our experiments show that FZL is exclusively localized to the inner envelope. This, together with trypsin protease treatment experiments by Gao et al., suggest that the GTPase domain and the coiled–coiled domain are exposed on the stromal side. Therefore, FZL could mediate vesicle fission

at the inner envelope membrane. However, the postulated role of FZL in membrane fission does not agree with the increased number of vesicles seen in *fzl* chloroplast by Gao et al. (2006). Yet, no vesicle accumulation could be seen in the electron micrographs shown by Tremblay et al. (2016). Moreover, we found none of the known or predicted chloroplast vesicle trafficking proteins were found to be dysregulated at least in the transcriptomic study, thus FZL could be a novel factor. This discrepancy could arise from various factors including the developmental stage of leaf, age of plants, or growth conditions, thus requiring more detailed investigation (Gugel and Soll 2017).

Overall, our results indicate that although FZL is located solely to the inner envelope of chloroplasts, it affects the maintenance of thylakoid membranes and consequently the function of photosynthetic complexes. Loss of FZL causes reduced photosynthetic efficiency and alters the stability of the cytochrome b_6f complex, especially in the midvein region of the leaves. Further experiments analysing the molecular mechanism of FZL need to be performed to elucidate the protein's specific role in thylakoid remodelling.

Materials and methods

Plant material and growth conditions

Three independent T-DNA insertion *fzl* lines (*fzl-1*: SALK_118335, *fzl*-2: SALK_033745C and *fzl-3*: SALK_152584C) were purchased from the European *Arabidopsis* Stock Centre (NASC, USA). Homozygous *fzl* lines were backcrossed with Col-0 and respective homozygous and WT lines were isolated in the T2 progeny. The presence of T-DNA insertions in exon 1 (SALK_118335), exon 2 (SALK_033745C) and exon 4 (SALK_152584C) was confirmed by sequencing. Plants were grown on soil under either under LED light (22 °C, 200 µmol m^{-2} s^{-1} light, 16/8 h light/dark) or in standard light conditions (22 °C, 100 µmol m^{-2} s^{-1} light, 16/8 h light/dark) as specified.

Spectroscopic analysis of chlorophyll fluorescence, P700 redox state and P700 re-reduction

Chlorophyll fluorescence of dark-adapted plants was recorded at RT using the MINI version of the Imaging PAM with an absorptance of 85% (Walz, Effeltrich). The area of interest in the mid-vein region was selected based on digital images of leaves, and Fv/Fm ratios were determined to quantify photosynthetic performance. Light curves were obtained using successive 20-s periods of illumination at increasing light intensities to calculate electron transfer rates through PSII [ETR] as well as qN with the aid of the ImagingWin software (Walz, Effeltrich) (Schreiber 1986). PSI absorbance changes at 820 nm were recorded with a DUAL-PAM-100 (Walz, Effeltrich). Oxidized P700 (ΔA_{max}) was recorded during far-red light illumination. The level of oxidized P700 in the leaf (ΔA) was determined during actinic light illumination (200 µmol photons m^{-2} s^{-1}). P700 re-reduction kinetics in the dark were recorded after oxidation of P700 by short illumination with far-red light. The half-time of the decay was calculated.

Protein expression analysis by SDS-PAGE

Plant material from WT and *fzl* mutants suspended in homogenization buffer [10 mM EDTA, 2 mM EGTA, 50 mM Tris/HCl (pH 8), 10 mM DTT] was homogenized using a micro pestle to extract proteins. After filtration through two layers of gauze, soluble and membrane protein fractions were separated by centrifugation for 10 min at 10,000 rpm at 4 °C. The samples were solubilized in SDS sample buffer and separated on a SDS polyacrylamide gel, blotted on a polyvinylidene difluoride membrane (PVDF), incubated with the appropriate primary antibody (supplementary table), and developed with enhanced chemiluminescence as previously described (Schwenkert et al. 2006). Purified at FZL (486–770 aa) protein was injected into rabbits and a polyclonal antiserum was generated to detect endogenous FZL protein (Pineda antibodies, Berlin). Antisera for D1, CoxII, Cyt*f*, PsaF, CP47 and LHCPs were obtained from Agrisera (Lund, Sweden). Antisera against TPI, GAPC-1 and SDH4 were obtained from Phytolab (Vestenbergsgreuth, Germany). $Cytb_6$ and CF_1-α/-β antisera were kind gift from Jörg Meurer, as were G6PDH Antisera from Antje von Schaewen. All other antisera are described elsewhere: Toc64 (Schweiger et al. 2012), Tic110 (Lubeck et al. 1996), FBPase (Benz et al. 2009), and PORB (Philippar et al. 2007).

Analysis of protein complexes by BN-PAGE

BN-PAGE was performed using samples prepared from WT and homozygous *fzl* plants grown under LED light as described in Urbischek et al. (2015).

Transcriptomic profiling using Affymetrix ATH1 microarray

For microarray analysis, leaves of 10 and 13-day F-old *fzl* (SALK_118335) plants grown on soil under LED light with light intensities of 200 µmol m^{-2} s^{-1}, photoperiod 16/8 h were used. To provide biological replicates, three samples were harvested from 10 individual plants. Total RNA was extracted with the Plant RNeasy Extraction kit (Qiagen). RNA concentration and purity were determined. The purified RNA (200 ng) was used to produce biotinylated cRNA

probes by using Affymetrix 3'-IVT Express kit (Affymetrix, High Wycombe, UK) according to the manufacturer's instructions. A total of 15 µg biotinylated cRNA was fragmented and hybridized to GeneChip *Arabidopsis* ATH1 arrays containing 22,810 probe sets. Washing and staining were done on an Affymetrix GeneChip Fluidics Station 450. The array chips were scanned using an Affymetrix GeneArray Scanner 3000. Raw signal intensity values (CEL files) were computed from the scanned array images using the Affymetrix GeneChip Command Console 3.0. For quality check and normalization, the raw intensity values were processed with Robin software default settings (Lohse et al. 2010). For background correction, the robust multiarray average normalization method was performed across all arrays (Irizarry et al. 2003). Statistical analysis of differential gene expression was carried out using the linear model-based approach developed by (Smyth 2004). The obtained P values were corrected for multiple testing using the strategy described by Benjamini and Hochberg (1995) separately for each of the comparisons made. Genes that showed a log2 fold-change value of at least 1 and a P value <0.05 were considered to be significantly differentially expressed. The significantly expressed genes were functionally annotated using Mapman BINs (Usadel et al. 2009).

In silico analysis of FZL

The Phyre2 program was used for in silico structural modelling. The FZL (288–912 aa) sequence was used as the query and analysis was run in intensive mode. PyMOL software was used to visualize the PDB output files obtained.

Chloroplast diameter measurements

Leaves from *fzl* and the respective outcrossed WT lines grown in normal light conditions (22 °C, 100 µmol m^{-2} s^{-1} light, 16/8 h light/dark) for 21 days were used for imaging using confocal laser scanning microscope from Leica, Type: TCS SP5. Imaging was done as described in Schweiger and Schwenkert (2014) to detect chlorophyll auto fluorescence. Diameters of at least 50 chloroplasts were measured using Fiji ImageJ software.

Chlorophyll measurements

For plants grown under LED light, chlorophyll was isolated as described previously using dimethylformamid (Porra et al. 1989). For plants grown under normal light chlorophyll isolation was performed in green light as described by Lichtenthaler and Wellburn (1983). Absorbance at 645, 663 and 750 nm was measured and chlorophyll concentrations were determined as described by Arnon (1949).

Acknowledgements This project was funded by the Deutsche Forschungsgemeinschaft (DFG), TR175, Project B05 to J.S. and SFB1035, Project A04 to S.S. F.S. was financially supported by Rhenac Green Tec AG (Hennef, Germany) for some time of the conducted study. We would like to thank Sabine Grahl for data analysis and help with supervision. Antje von Schaewen and Jörg Meurer are kindly acknowledged for providing antisera. We would further like to thank Chris Carrie and his group for providing isolated mitochondria.

References

Arnon DJ (1949) Copper enzymes in isolated chloroplasts. Polyphenoloxidase in *Beta vulgaris*. Plant Physiol 24:1–15

Benjamini Y, Hochberg Y (1995) Controlling the false discovery rate: a practical and powerful approach to multiple testing. J R Stat Soc 57:289–300

Benz JP et al (2009) Arabidopsis Tic62 and ferredoxin-NADP(H) oxidoreductase form light-regulated complexes that are integrated into the chloroplast redox poise. Plant Cell 21:3965–3983. https://doi.org/10.1105/tpc.109.069815

Charuvi D, Kiss V, Nevo R, Shimoni E, Adam Z, Reich Z (2012) Gain and loss of photosynthetic membranes during plastid differentiation in the shoot apex of Arabidopsis. Plant Cell 24:1143–1157. https://doi.org/10.1105/tpc.111.094458

Gao H, Sage TL, Osteryoung KW (2006) FZL, an FZO-like protein in plants, is a determinant of thylakoid and chloroplast morphology. Proc Natl Acad Sci USA 103:6759–6764. https://doi.org/10.1073/pnas.0507287103

Gugel IL, Soll J (2017) Chloroplast differentiation in the growing leaves of Arabidopsis thaliana. Protoplasma 254:1857–1866. https://doi.org/10.1007/s00709-016-1057-9

Hojka M, Thiele W, Toth SZ, Lein W, Bock R, Schottler MA (2014) Inducible repression of nuclear-encoded subunits of the cytochrome b6f complex in tobacco reveals an extraordinarily long lifetime of the complex. Plant Physiol 165:1632–1646. https://doi.org/10.1104/pp.114.243741

Irizarry RA, Hobbs B, Collin F, Beazer-Barclay YD, Antonellis KJ, Scherf U, Speed TP (2003) Exploration, normalization, and summaries of high density oligonucleotide array probe level data. Biostatistics 4:249–264. https://doi.org/10.1093/biostatistics/4.2.249

Jilly R, Khan NZ, Aronsson H, Schneider D (2018) Dynamin-like proteins are potentially involved in membrane dynamics within chloroplasts and cyanobacteria. Front Plant Sci 9:206. https://doi.org/10.3389/fpls.2018.00206

Karim S, Aronsson H (2014) The puzzle of chloroplast vesicle transport—involvement of GTPases. Front Plant Sci 5:472. https://doi.org/10.3389/fpls.2014.00472

Landoni M et al (2013) A mutation in the FZL gene of Arabidopsis causing alteration in chloroplast morphology results in a lesion mimic phenotype. J Exp Bot 64:4313–4328. https://doi.org/10.1093/jxb/ert237

Lichtenthaler H, Wellburn A (1983) Determinations of total carotenoids and chlorophylls a and b of leaf extracts in different solvents. Biochem Soc Trans 11:591–592

Lohse M et al (2010) Robin: an intuitive wizard application for R-based expression microarray quality assessment and analysis. Plant Physiol 153:642–651. https://doi.org/10.1104/pp.109.152553

Low HH, Lowe J (2006) A bacterial dynamin-like protein. Nature 444:766–769. https://doi.org/10.1038/nature05312

Low HH, Sachse C, Amos LA, Lowe J (2009) Structure of a bacterial dynamin-like protein lipid tube provides a mechanism for assembly and membrane curving. Cell 139:1342–1352. https://doi.org/10.1016/j.cell.2009.11.003

Lubeck J, Soll J, Akita M, Nielsen E, Keegstra K (1996) Topology of IEP110, a component of the chloroplastic protein import machinery present in the inner envelope membrane. EMBO J 15:4230–4238

Mozdy AD, Shaw JM (2003) A fuzzy mitochondrial fusion apparatus comes into focus. Nat Rev Mol Cell Biol 4:468–478. https://doi.org/10.1038/nrm1125

Philippar K, Geis T, Ilkavets I, Oster U, Schwenkert S, Meurer J, Soll J (2007) Chloroplast biogenesis: the use of mutants to study the etioplast-chloroplast transition. Proc Natl Acad Sci USA 104:678–683. https://doi.org/10.1073/pnas.0610062104

Porra RJ, Thompson WA, Kriedemann PE (1989) Determination of accurate extinction coefficients and simultaneous equations for assaying chlorophylls a and b extracted with four different solvents: verification of the concentration of chlorophyll standards by atomic absorption spectroscopy. Biochim. Biophys. Acta 975:384–394

Schottler MA, Flugel C, Thiele W, Bock R (2007) Knock-out of the plastid-encoded PetL subunit results in reduced stability and accelerated leaf age-dependent loss of the cytochrome b6f complex. J Biol Chem 282:976–985. https://doi.org/10.1074/jbc.M606436200

Schottler MA, Toth SZ, Boulouis A, Kahlau S (2015) Photosynthetic complex stoichiometry dynamics in higher plants: biogenesis, function, and turnover of ATP synthase and the cytochrome b6f complex. J Exp Bot 66:2373–2400. https://doi.org/10.1093/jxb/eru495

Schreiber U (1986) Detection of rapid induction kinetics with a new type of high-frequency modulated chlorophyll fluorometer. Photosynth Res 9:261–272. https://doi.org/10.1007/BF00029749

Schweiger R, Schwenkert S (2014) Protein-protein interactions visualized by bimolecular fluorescence complementation in tobacco protoplasts and leaves. J Vis Exp. https://doi.org/10.3791/51327

Schweiger R, Muller NC, Schmitt MJ, Soll J, Schwenkert S (2012) AtTPR7 is a chaperone docking protein of the Sec translocon in Arabidopsis. J Cell Sci. https://doi.org/10.1242/jcs.111054

Schwenkert S et al (2006) PsbI affects the stability, function, and phosphorylation patterns of photosystem II assemblies in tobacco. J Biol Chem 281:34227–34238. https://doi.org/10.1074/jbc.M604888200

Schwenkert S, Legen J, Takami T, Shikanai T, Herrmann RG, Meurer J (2007) Role of the low-molecular-weight subunits PetL, PetG, and PetN in assembly, stability, and dimerization of the cytochrome b6f complex in tobacco. Plant Physiol 144:1924–1935. https://doi.org/10.1104/pp.107.100131

Smyth GK (2004) Linear models and empirical bayes methods for assessing differential expression in microarray experiments. Stat Appl Genet Mol Biol. https://doi.org/10.2202/1544-6115.1027

Tremblay A et al (2016) A role of the fuzzy onions like gene in regulating cell death and defense in Arabidopsis. Sci Rep 6:37797. https://doi.org/10.1038/srep37797

Urbischek M et al (2015) The extreme Albino3 (Alb3) C terminus is required for Alb3 stability and function in *Arabidopsis thaliana*. Planta 242:733–746. https://doi.org/10.1007/s00425-015-2352-y

Usadel B, Poree F, Nagel A, Lohse M, Czedik-Eysenberg A, Stitt M (2009) A guide to using MapMan to visualize and compare Omics data in plants: a case study in the crop species, Maize. Plant Cell Environ 32:1211–1229

van der Bliek AM, Shen Q, Kawajiri S (2013) Mechanisms of mitochondrial fission and fusion. Cold Spring Harb Perspect Biol. https://doi.org/10.1101/cshperspect.a011072

Waters MT, Langdale JA (2009) The making of a chloroplast. EMBO J 28:2861–2873. https://doi.org/10.1038/emboj.2009.264

Westphal S, Soll J, Vothknecht UC (2001) A vesicle transport system inside chloroplasts. FEBS Lett 506:257–261

Yamori W, Takahashi S, Makino A, Price GD, Badger MR, von Caemmerer S (2011) The roles of ATP synthase and the cytochrome b6/f complexes in limiting chloroplast electron transport and determining photosynthetic capacity. Plant Physiol 155:956–962. https://doi.org/10.1104/pp.110.168435